10-YEAR ANNIVERSARY SERIES

Proteins on the move: insights gained from fluorescent protein technologies

Atsushi Miyawaki

Abstract | Proteins are always on the move, and this may occur through diffusion or active transport. The realization that the regulation of signal transduction is highly dynamic in space and time has stimulated intense interest in the movement of proteins. Over the past decade, numerous new technologies using fluorescent proteins have been developed, allowing us to observe the spatiotemporal dynamics of proteins in living cells. These technologies have greatly advanced our understanding of protein dynamics, including protein movement and protein interactions.

In recent years, our ability to unravel the fine details of cellular events has improved remarkably. One significant contributing factor in this was the development of green fluorescent protein (GFP) from the jellyfish *Aequorea victoria* as a fluorescent label that can be incorporated into proteins by genetic fusion[1]. Chimeric GFPs can be expressed *in situ* by gene transfer into cells and localized to particular sites with appropriate targeting signals, thereby allowing imaging of a range of biological events. Furthermore, the emergence of spectral variants of *A. victoria* GFP, as well as the identification of GFP-like proteins from other organisms, has provided many new opportunities for investigators to simultaneously observe multiple cellular events[2–7].

In 2001, a review by Lippincott-Schwartz, Snapp and Kenworthy[8] provided an early perspective on these useful tools. Since then, there has been great progress. For example, inspired by previous studies of the photochemical transformation of wild-type *A. victoria* GFP[9,10] and by molecular cloning of GFP-like proteins from non-bioluminescent anthozoan species[11], Lippincott-Schwartz's group[12] and my own[13] developed a photoactivatable FP (PA-GFP) and a photoconvertible FP (Kaede), respectively; these FPs were introduced to the biological community in 2002. These technological innovations that date back to 2002 paved the way to notable advances in fluorescence imaging as applied to the observation of protein movement.

In commemoration of the 10-year anniversary of *Nature Reviews Molecular Cell Biology*, I revisit the review by Lippincott-Schwartz, Snapp and Kenworthy[8], which was published in the journal's first year (2001). Revisiting that original review provides us with an opportunity to reflect on new imaging approaches that are in use today but were inconceivable only a decade ago. Since 2001, *Nature Reviews Molecular Cell Biology* has covered numerous state-of-the-art fluorescence imaging technologies, with some of the articles focusing on the techniques in question[14–20] and others on applying these techniques to answer cell and molecular biology questions[21,22]. As the fluorescence imaging field has become increasingly diversified, it has become more and more of a challenge to exhaustively review all of these technologies. Therefore, here I focus on the techniques for visualizing protein movement, in particular diffusion (BOX 1). Other important biological events, such as protein–protein interactions, are also discussed in relation to this subject because they are closely related to protein movement. The fluorophores discussed in this Review are limited mostly to FPs, a term I use to describe proteins that can become spontaneously fluorescent through the autocatalytic synthesis of a chromophore[1]. In addition, the samples discussed here are mostly live cultured mammalian cells on coverslips. The *in vivo* imaging of cell behaviour in intact multicellular organisms has been reviewed elsewhere[23–25].

Labelling with GFP-like proteins

The family of GFP-like proteins has expanded rapidly and continues to grow[26–28]. Although GFP-like proteins exhibit a diverse set of features, they all share a few basic properties. For example, all of the wild-type GFP-like proteins characterized so far form obligate oligomers, whereas wild-type *A. victoria* GFP forms a weak dimer (with a dissociation constant of 0.11 mM)[29]. It is important to consider these properties when using GFP-like proteins as tags to analyse protein movement.

Life Function and Dynamics, Exploratory Research for Advanced Technology (ERATO), Japan Science and Technology Corporation (JST); and Laboratory for Cell Function and Dynamics, Brain Science Institute, RIKEN, 2-1 Hirosawa, Wako City, Saitama 351-0198, Japan.
e-mail: matsushi@brain.riken.jp
doi:10.1038/nrm3199

Box 1 | **Mechanisms of biomolecule movement**

There are two types of transport processes: non-mediated and mediated transport. Non-mediated transport occurs through simple diffusion, which is the result of thermal fluctuations in the suspension and is often referred to as Brownian motion. Mediated transport occurs through the action of specific carrier proteins and is classified into two categories depending on the thermodynamics of the system: facilitated diffusion and active transport. In facilitated diffusion, molecules flow from areas of high concentration to areas of low concentration to reach equilibrium. In active transport, molecules are transported from areas of low concentration to those of high concentration, against their concentration gradients. The transport of molecules across the nuclear envelope from the cytoplasm to the nucleus can be used as an example of these mechanisms. Steroid hormones pass through the membrane by simple diffusion. Small water-soluble proteins (<50 kDa) can pass through nuclear pore complexes (which perforate the nuclear envelope) by facilitated diffusion, whereas large proteins (>60 kDa) cannot. However, proteins containing nuclear localization signals (NLSs) can enter the nucleus irrespective of their size through active transport. The entire cycle of NLS-mediated protein transport requires GTP hydrolysis and is therefore energy dependent. Other examples of active transport include the directed movement of proteins, mRNAs and vesicles along cytoskeletal elements, which is mediated by motor proteins.

Oligomerization of GFP-like proteins. Oligomerization does not limit the ability of GFP-like proteins to mark cells or act as reporters of gene expression, but it may interfere with the function of the protein to which they are fused. Therefore, many groups have attempted to engineer monomeric FPs (mFPs). Tsien's group reported the successful engineering of monomeric red FP1 (mRFP1)[30] from *Discosoma* spp. RFP (DsRed)[11], a molecule that normally forms a tetramer[31,32] (FIG. 1a). They used site-directed mutagenesis to break the tetrameric structure, followed by random mutagenesis to rescue the red fluorescence. Following their success with mRFP1, the group carried out an extensive series of *in vitro* evolution experiments, generating a 'virtual fruit basket' of FPs with a wide range of emission spectra[33], including mCherry and mOrange. These achievements demonstrate the potential for the development of monomeric forms of other oligomeric FPs.

It should also be noted that Tsien's group fused two copies of the DsRed-derived dimer (joined at the AC interface) using a polypeptide linker (FIG. 1a). In such a tandem dimer construct, key dimer interactions can be satisfied through intramolecular contacts. The latest version of the protein is tandem dimeric Tomato (tdTomato)[33], which has been widely used because it doubles the fluorescence brightness per unit of host protein compared with the regular monomer and is thus preferable when the size of the fusion tag is not a significant concern. Another example is tdEosFP, which was developed from an AB dimer of the tetrameric complex of EosFP[34] and has been widely used for super-resolution microscopy techniques, such as photoactivated localization microscopy (PALM) and fluorescence PALM (FPALM) (see below).

Aggregation of GFP-like proteins. The tendency of anthozoan GFP-like proteins to form aggregates is another important consideration. After cells are transfected with cDNAs encoding these GFP-like proteins, visible precipitates (assumed to be protein aggregates) appear in the cytoplasm[35]. Because the aggregation of FPs may impede cellular applications and lead to toxicity, most cell biologists refrain from using FPs that form visible cytosolic precipitates[35] and tend to discuss aggregation and oligomerization of GFP-like proteins as though they were synonymous. Importantly, however, my group has observed visible precipitates with non-fused GFP-like proteins, regardless of their degree of oligomerization[36]; for example, the transfection of non-fused mRFP1 into HeLa cells produced visible precipitates in the cytosol[36]. Such observations prompted us to investigate the nature of these cytosolic precipitates to determine how they are formed and whether FPs that form such precipitates should be avoided. Using cytochemical and biochemical approaches, we showed that the visible precipitates in the cytoplasm are lysosomes that have accumulated GFP-like proteins[36]. Most GFP-like proteins are resistant to both acid and lysosomal enzymes and therefore retain their fluorescence in lysosomes. By contrast, *A. victoria* GFP and its derivatives, such as enhanced GFP (EGFP), enhanced cyan FP (ECFP) and enhanced yellow FP (EYFP), are degraded rapidly in lysosomes[36]. Thus, the visible precipitates in cells transfected with cDNAs encoding GFP-like proteins could be the products of cytoprotective, rather than cytotoxic, responses.

However, lysosomal accumulation of FPs cannot explain all instances of visible precipitates, as FP aggregation does occur in some situations. Although the molecular mechanisms of FP aggregation remain unclear, two possibilities deserve attention. First, the aggregation may take place through electrostatic or hydrophobic interactions between FP oligomeric complexes (FIG. 1b). These FPs can aggregate regardless of whether they are fused to host proteins. In fact, it is possible to engineer non-aggregating FPs by removing charged or hydrophobic side chains from the surfaces of oligomeric complexes[35]. It should be noted that GFP from the sea pansy *Renilla reniformis* becomes soluble as a result of dimerization; a hydrophobic patch is concealed at the dimerization interface, which allows the overall surface of the dimer to be hydrophilic. This principle also applies to some tetrameric GFP-like proteins, such as Kaede[13] and KikGR[37], which exhibit higher than expected (given their molecular masses) diffusion coefficients within the cytoplasm (see below), indicative of high solubility[13,38].

Second, aggregation may be a consequence of FP oligomerization. If host proteins are also oligomeric, fusion to FPs may result in crosslinking to form massive aggregates[39] (FIG. 1c). However, such large-scale aggregation should occur only when the FPs are fused to other proteins. If oligomerization precedes aggregation then this problem would be most easily solved by using mFPs. Nevertheless, it seems to be hard to make monomeric forms of some GFP-like proteins, so another solution may be to carry out hetero-oligomeric tagging, which supplies an FP-tagged protein with an excess of free, non-fluorescent mutants of the FP[40].

Site-directed mutagenesis
An *in vitro* mutagenesis procedure that is often carried out using a polymerase chain reaction in which specific mutations are introduced into a DNA molecule.

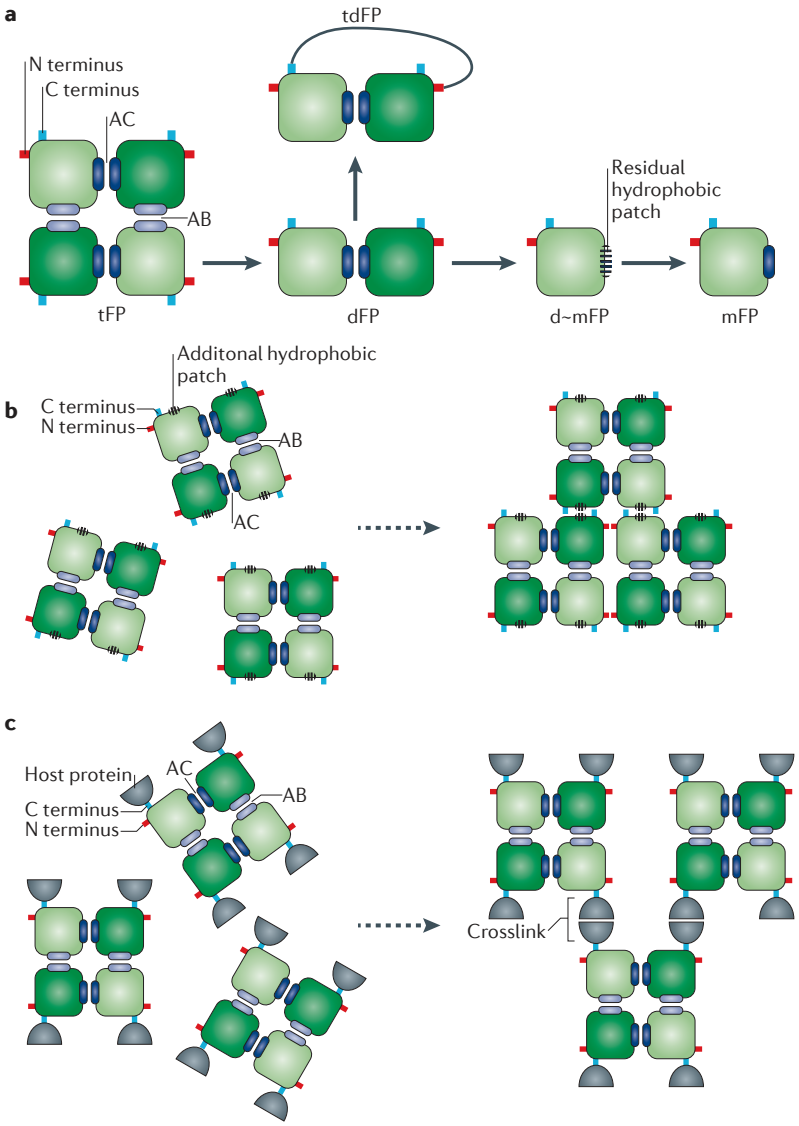

Figure 1 | **Oligomerization and aggregation of GFP-like proteins. a** | Construction of fluorescent proteins (FPs) for protein fusion from a tetrameric FP (tFP). Despite only modest sequence identity with *Aequorea victoria* green FP (GFP), GFP-like proteins share a β-can fold (an 11-stranded β-barrel), which is shown as a rounded square of light green (top view) or dark green (bottom view). Each subunit has an amino terminus and a carboxyl terminus. In a tFP, each subunit has two hydrophobic patches on its surface. The patches drawn in grey and blue constitute the AB and AC interfaces, respectively. Elimination of the hydrophobic patch at the AB interface in tFP generates an AC dimeric FP (dFP). By linking the C terminus of A and the N terminus of C, it is possible to generate a tandem dimeric FP (tdFP) from a dFP. Elimination of the hydrophobic patch at the AC interface of the dFP generates a monomeric FP (mFP). Incomplete elimination results in the generation of an 'incomplete monomer' (d~mFP; in which the '~' represents ambiguity about the monomerization), which is not suitable for use as a fusion tag. **b** | An additional hydrophobic patch on the free surface of the subunit contributes to the generation of a tFP aggregate. **c** | Fusion to oligomeric host proteins may lead to the formation of large aggregates owing to crosslinking of the host proteins.

Measuring bulk mass movement

Assuming that neither fusion with FP nor overexpression of FP-fused proteins affects protein dynamics inside cells, we can study how the FP-fused proteins move by measuring fluorescence from an ensemble (or bulk collection) of proteins.

Hydrodynamic radius
The effective size of the molecule as detected by its diffusion.

Protein diffusion in living cells. Diffusion is the overall movement of material from an area of high concentration to an area of low concentration. The diffusion constant, *D*, represents the rate of protein movement in the absence of flow or active transport (BOX 1). According to the Stokes–Einstein formula, *D* for a particle in a free volume is determined by the absolute temperature, the viscosity of the medium and the hydrodynamic radius of the particle. In live biological samples, the absolute temperature is almost always constant and is therefore not relevant. By contrast, the viscosity is a variable. As membranes are more viscous than aqueous phases (such as the cytoplasm, nucleoplasm and organelle lumina), the lateral diffusion of a membrane protein is slower than that of a soluble protein. In addition, the *D* for a soluble globular protein is inversely proportional to the cube root of the protein's molecular mass.

Within a cell, however, free diffusion of a protein can be hindered by its interactions with other proteins and structures. In a crowded environment, a protein often interacts with other mobile proteins and can bind to relatively immobile cellular structures, such as the cytoskeleton, chromatin and plasma membrane. Either way, the protein in question moves more slowly than would be expected for its size. Moreover, a fraction of the protein molecules (termed the immobile fraction) is assumed to be trapped during the time of observation by binding to immobile cellular structures. These two kinetic parameters of a protein — the apparent *D* and the immobile fraction — can be extracted from the data of bulk mass movement measurements[41–45]. It is important to note that, owing to macromolecular crowding, there are situations in which diffusion cannot be described in terms of a single *D* value (BOX 2).

Photobleaching-based measurements. The movement of FP-fused proteins has been assessed conventionally using photobleaching techniques, such as fluorescence recovery after photobleaching (FRAP) and fluorescence loss in photobleaching (FLIP). In both techniques, fluorescent molecules in a certain region of the cell are irreversibly photobleached with a high-power laser beam, which allows observation of the surrounding non-bleached fluorescent molecules into the photobleached region. In the FRAP technique, fluorescence recovery is monitored in the bleached region after photobleaching (FIG. 2a–d). By contrast, in the FLIP technique, fluorescence loss is monitored in the unbleached region during photobleaching. Thus, the two techniques are, in a sense, complementary.

Each of these techniques usually yields a series of confocal images that allows one to determine whether free diffusion is blocked within the cellular structure where an FP-fused protein is localized (compartment connectivity)[43,45–49], which may also yield information about the structure itself. For example, analysis of FRAP data in the endoplasmic reticulum (ER) suggested that free diffusion is permitted[43], which highlights the connectivity of the ER structure. In addition, temporal profiles of fluorescence intensities in FRAP or FLIP data provide descriptive parameters, such as the mobile and

Box 2 | **Anomalous diffusion**

In anomalous diffusion, the diffusion constant, *D*, is not constant but changes with time (*D*(*t*)) and/or space (*D*(*x*, *y*, *z*)). This phenomenon has been observed both *in vitro* and in living cultured cells[137]. A range of physical mechanisms has been proposed to explain how diffusion can be anomalous and influenced by other factors. For example, inside the endoplasmic reticulum (ER), the diffusion of misfolded proteins is affected by their interaction with the ER quality control machinery[138]. Also, inside dense nuclear compartments, molecular crowding was found to affect the diffusion and binding of nuclear proteins in heterochromatin. Observing anomalous diffusion can offer useful insights; a fractal model of chromatin organization was proposed by observing the behaviour of nuclear proteins[139].

immobile fractions, as well as the halftime of recovery (using FRAP) or loss (using FLIP) of fluorescence, which can be used to calculate the apparent *D*.

In addition to the diffusional properties of the analysed protein, the biophysical properties of the immobile fraction, such as the association and dissociation rates (ON and OFF rates) from localized binding sites, can be extracted by a combination of kinetic modelling and computer simulation. When diffusion is fast compared with association–dissociation processes, a compartmental computational model[45] using ordinary differential equations can be used under the assumption that the analysed proteins are quickly mixed within each compartment (diffusion-uncoupled FRAP)[44]. However, when association–dissociation processes and diffusion occur on similar timescales, the spatiotemporal dynamics of the protein is limited by diffusion as well (diffusion-coupled FRAP)[44]. In such cases, spatial modelling[45] that uses partial differential equations (with more than one independent variable) is preferable to take diffusion-related parameters into account and allow more accurate kinetic modelling. One can estimate how the observed binding pattern is limited by diffusion by comparing the time course of recovery (using FRAP) or loss (using FLIP) in different parts of a compartment.

One major drawback of the photobleaching techniques is their inability to analyse fast diffusion (for example, of proteins with an apparent *D* as large as 100 $\mu m^2 s^{-1}$), although some approaches have been described that reduce this limitation[50–52] (see below). This is because these techniques necessitate full photobleaching, which requires relatively long and intense illumination in a specific region of the cell. Accordingly, photobleaching techniques have mostly been useful for measuring the slow movements of proteins within a membrane, which have an apparent *D* that is below 1 $\mu m^2 s^{-1}$.

Photoactivation- and photoconversion-based measurements. Photobleaching techniques have recently been replaced with or complemented by photoactivation or photoconversion experiments, which use photomodulatable FPs. Since 2002, numerous photoactivatable FPs have been developed (see Supplementary information S1 (figure)) (reviewed in REFS 17,53,54). Examples include a PA-GFP derived from *A. victoria* GFP[12], many PA-RFPs (including PA-mRFP1s[55], PA-mCherry[56] and PA-TagRFP[57]) and a photoactivatable fluorescence resonance energy transfer (FRET) probe (Phamret)[58] that induces a change in fluorescence emission from ECFP to photoactivated PA-GFP when irradiated with violet light. In addition, photoconvertible FPs for use in protein fusions have been generated. tdEosFP, mEosFP[59], mKikGR[60], Dendra2 (REF. 61) and mIrisFP[62] show green-to-red photoconversion. An interesting pair is the cyan-to-green photoswitchable CFP2 (PS-CFP2)[63] and orange-to-far-red PS-mOrange[64], which are photoconverted by violet light and blue-green light, respectively, and can be used to differentially highlight two distinct proteins and simultaneously image both the converted and unconverted populations of each.

Hereafter, the term photoactivation will include photoconversion as well. Photoactivatable FP-fused proteins can be optically labelled by partial photoactivation using unique colour markers that require faster and less intense light exposure than photobleaching, thus allowing measurements of fast protein movements with an apparent *D* as large as 100 $\mu m^2 s^{-1}$ (FIG. 2e–h). Photoactivation is usually done by locally irradiating a region of interest within a cell with a very short pulse of violet light. By monitoring the decay of the emerging fluorescence, one can analyse the dissociation rates of local protein binding. By contrast, conventional FRAP techniques can provide information about the association rates. For example, the binding kinetics of the tethering factor early endosome antigen 1 (EEA1) was analysed through photoactivation and FRAP experiments that used EEA1–PA-EGFP and EEA1–EGFP, respectively[65]. Although these comparative studies were descriptive, they revealed that the association rate of EEA1 with the endosomal membrane was much faster than the dissociation rate, and that the residence time of EEA1 on the endosomal membrane was determined by the dissociation rate. In addition to elucidating the thermodynamics of protein binding, determining of the association and dissociation rates offers information on the kinetics of protein binding. For example, a recent study used a fluorescence decay after photoactivation (FDAP) assay to examine the binding kinetics of the pluripotency factor OCT4 and observed that the kinetics of chromatin binding of OCT4 predicts cell lineage patterning in the early mouse embryo[66].

Protein dynamics inside dendritic spines. Photoactivation and photobleaching techniques have been used to examine the kinetics of protein movement within dendritic spines. Initially, the chemical compartmentalization between dendritic spines and shafts was examined by two-photon photobleaching and photorelease of fluorescein–dextran[67]. Two-photon microscopy is generally characterized by the intrinsic spatial confinement of excitation[68]. Because it cannot generate instantaneous and complete bleaching in a large three-dimensional (3D) space, the two-photon approach seems to be generally inadequate for FRAP. However, as dendritic spines are very small, with head volumes ranging from 0.01 μm^3 to 0.8 μm^3, they can be examined using the two-photon photobleaching technique[69].

Fractal model
A model in which diffusing molecules and complexes encounter the same obstructions regardless of their size.

Dendritic spines
Small membranous protrusions from dendritic shafts that usually receive excitatory input.

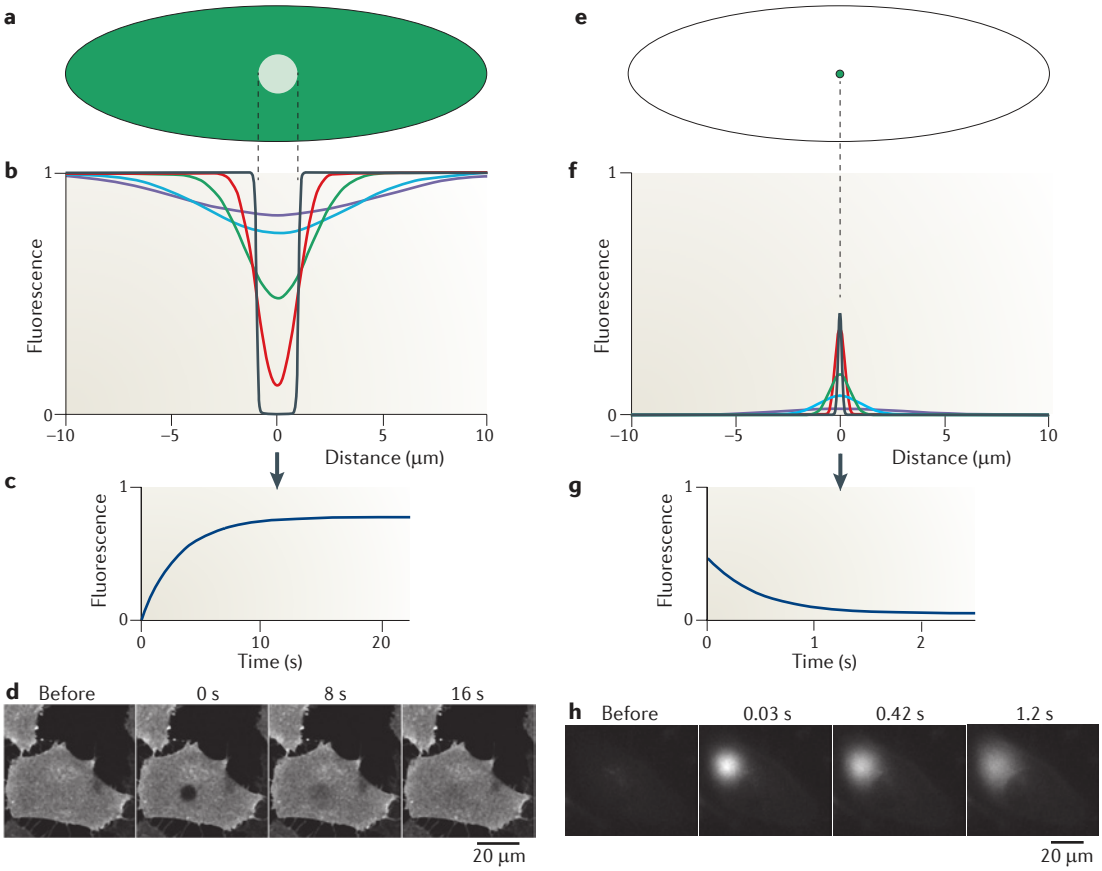

Figure 2 | **Relaxation processes after photobleaching and photoactivation. a** | In photobleaching, the cell is modelled as a flattened, homogenous cylinder with a radius of 10 μm, which is filled with enhanced green fluorescent protein (EGFP). **b** | Fluorescence–distance curves. Assuming that instantaneous and complete bleaching is achieved by intense 488-nm laser illumination in a small cylinder, the figure shows how the EGFP fluorescence distribution along the line in **a** relaxes towards the steady state. **c** | Fluorescence recovery at the centre of the bleached region. **d** | A series of images of a HeLa cell expressing Lyn-Venus, a membrane-bound variant of yellow FP (YFP), which were acquired using a confocal laser-scanning microscope after photobleaching (tornado scan). **e** | In photoactivation, the modelled cell is filled with photoactivatable GFP (PA-GFP) and briefly illuminated at one spot by a short pulse from a 405-nm laser. **f,g** | Fluorescence–distance curves (**f**) and the fluorescence activation at the centre of the spot (**g**) are shown. **h** | A series of images of a HeLa cell expressing Kaede in the cytosol, which were acquired using conventional wide-field microscopy. A pinhole was placed in the plane of the field iris in the ultraviolet (UV) illuminator to focus the UV pulse on a spot 10 μm in diameter. Red fluorescence images were taken about every 0.1 seconds. A spot of red fluorescence emerged 0.03 seconds after the UV pulse, which spread concentrically until it reached the nuclear envelope at 1.2 seconds. Images in part **h** are reproduced, with permission, from REF. 13 © (2002) National Academy of Sciences, USA.

In particular, numerous studies have focused on the actin cytoskeleton (which regulates the structure and plasticity of a dendritic spine), and many of these have used actin–EGFP[70]. For example, the rapid turnover of actin in dendritic spines, and its activity-dependent regulation, were observed by carrying out conventional FRAP on dissociated hippocampal neurons expressing actin–EGFP. In many of these photobleaching experiments, however, the dendritic spine was regarded as a homogenous compartment. Conversely, using two-photon photoactivation of β-actin fused to PA-GFP, one study successfully identified three filamentous actin (F-actin) pools that contributed differentially to spine enlargement and probably also to plasticity[71]. This was achieved by directly visualizing the flow of F-actin pools inside individual dendritic spines on CA1 pyramidal neurons in rat hippocampal slices. Owing to the unique features of two-photon photoactivation, the researchers were able to achieve 3D-confined highlighting of F-actin and thus investigate actin dynamics with satisfactorily high spatial and temporal resolutions within a dendritic spine. The combination of PA-GFP and two-photon photoactivation was also applied to studies of the dynamics of postsynaptic density 95 (PSD95; also known as DLG4), a member of the membrane-associated guanylate kinase family of scaffolding proteins, within individual spines in dendrites of layer 2 or 3 pyramidal neurons in the developing mouse barrel cortex[72], as well as in hippocampal neurons in rat organotypic slices[73]. In these cases, the two-photon photoactivation technique allowed the elucidation of 3D protein movement, which could not, in principle, be achieved by conventional (one-photon) photobleaching experiments.

Pyramidal neurons
The predominant type of neuron in the neocortex. They are named after their triangular cell bodies.

Barrel cortex
The dark-staining regions of layer 4 of the somatosensory cortex, where somatosensory inputs from the contralateral side of the body come in from the thalamus.

Photobleaching versus photoactivation. Both photobleaching and photoactivation have provided great insights into the speed of diffusion and the association–dissociation rates of proteins. The choice of technique will depend on the speed of diffusion of an FP-fused protein relative to the rates of the protein's binding process and the FP's photobleaching–photoactivation process. If protein diffusion is slow compared with the binding kinetics, the spatiotemporal pattern of the output will also be limited by diffusion; in this case, spatial modelling using partial differential equations (see above) should be used, taking into account the precise value of the apparent *D*. However, to be quantified, the apparent *D* must be slower that the photobleaching or photoactivation of the FP. Because photoactivation is usually more efficient than photobleaching, and because only partial photoactivation is needed to generate an instantaneous fluorescence source (FIG. 2), the photoactivation time can be significantly shortened for the measurement of large apparent *D* values. Therefore, if the diffusion process is fast compared with the photobleaching of the FP, photoactivation is preferred and a photoactivatable FP should be used.

Before the advent of photoactivatable FPs, Verkman's group[50–52] designed elaborate instrumentation and analytic methods based on photobleaching for bulk (FRAP) measurements of fast diffusion ($D = 5–30\ \mu m^2\ s^{-1}$) of bright variants of *A. victoria* GFP in aqueous compartments, such as the cytoplasm[50], the mitochondrial matrix[51] and the ER[52]. However, FRAP measurements of diffusion were more easily carried out on EGFP-fused proteins diffusing within biological membranes[8] (through slow diffusion). Photobleaching techniques could monitor their slow lateral diffusion in the membranes, which could also be effectively characterized by the 2D diffusion of a molecule in a thin and flat medium. Today, photoactivation techniques in combination with two-photon excitation have improved not only the temporal resolution of diffusion analyses but also the spatial resolution of 3D diffusion analyses in the aqueous phase.

Reversible photoswitching (photochromism). The irreversibility of the photobleaching and photoactivation techniques prevents recurrent monitoring of the same protein in a study of its temporal regulation. This problem can be solved by using reversibly photoswitchable (photochromic) FPs, such as FP595 (REF. 74), kindling FP1 (KFP1)[75], Dronpa[76] and its derivatives[77], Padron[78], monomeric teal FP 0.7 (mTFP0.7)[79], IrisFP[80], reversibly switchable Cherry (rsCherry)[81], rsCherryRev[81] and rsTagRFP[82]. Dronpa, for example, is a green-light-emitting, monomeric and photochromic FP with excellent bright/dark contrast. The photochromic characteristics of these FPs enable studies of fast protein dynamics at multiple time points in individual cells. For example, by repeatedly labelling the same regions, it was possible to observe the real-time flow of mitogen-activated protein kinase (MAPK) across the nuclear envelope, demonstrating that the kinase's nucleocytoplasmic shuttling rate increased following growth factor stimulation[76].

Effects of FP fusion and overexpression. It is possible that the diffusion of a free protein differs from that of the same protein fused to an FP. Indeed, fusion with an FP should have some measurable effects on the protein, including changes in size or the propensity to bind other proteins or structures. In this context, I am more concerned about changes in binding patterns. Ideally, the surface of an FP should be completely hydrophilic to ensure that they do not bind other structures. However, although many GFP-like proteins have been successfully made into monomeric forms, there may be also 'incomplete monomers' (dimeric~mFPs (d~mFPs); in which the '~' represents ambiguity about the monomerization) (FIG. 1a), which have sticky, hydrophobic patches on their surfaces. When this type of FP is used, the diffusion of the FP-fused protein will be slowed down, and in fact d~mFPs themselves show substantially slower diffusion in their free form than mFPs (A.M., unpublished observations).

Moreover, the measurement of bulk mass movement usually requires that cells and subcellular structures be loaded with high levels of FP-fused proteins to maintain a good signal/noise ratio. However, the high expression levels of FP-fused proteins may perturb normal cellular processes and produce artefactual movement owing to the relatively lower levels of binding partners inside cells. Therefore, when interpreting data from such experiments, a great deal of care should be taken in consideration of the relative amounts of FP-fused proteins and endogenous proteins[83,84].

Measurements of single-molecule movement

In contrast to bulk measurements, measurements of single-molecule movement mainly record the trajectories of individual proteins by tracking them in the cell. A range of techniques has been developed to label and track single proteins, and these methods are discussed below.

Tracking membrane surface proteins. Conventionally, surface proteins are analysed by labelling with colloidal gold particles and visualized using differential interference contrast microscopy[85]. Alternatively, those proteins can be labelled with chemical fluorophores or quantum dots (BOX 3) and visualized by fluorescence microscopy[86]. Because endogenous proteins in the plasma membrane have accessible extracellular domains, they can be labelled using specific antibodies conjugated with colloidal gold particles, chemical fluorophores or quantum dots rather than FPs.

Analyses of individual membrane proteins have yielded insights into protein movement, as well as the structure of the membrane itself. For example, by analysing translational diffusion of transmembrane proteins and glycosyl phosphatidylinositol (GPI)-anchored proteins, one study showed that the plasma membrane is partitioned into compartments that are 50–300 nm wide[87]. These compartments are constructed by actin-based membrane skeleton 'fences', with the anchored transmembrane proteins acting as 'pickets'. Accordingly, membrane proteins are highly mobile and exhibit random walk trajectories within their compartments, but 'hop' across the fences only infrequently. This infrequent hopping

Box 3 | **Organic fluorophores and quantum dots**

Although this Review focuses on techniques that use fluorescent proteins (FPs), there have also been various recent advances in techniques for labelling proteins with other fluorophores. One disadvantage of FPs is that they are large tags (~27 kDa in monomeric form). The use of small organic fluorophores, such as fluorescein and rhodamine (<1 kDa) can minimize possible steric hindrance problems that interfere with protein function, and site-specific attachment of the fluorophores to proteins may allow the assessment of changes in local environments. More and more innovative techniques have been developed recently[140], including bi-arsenic fluorophore labelling of proteins that have been genetically altered to contain tetracysteine motifs, labelling of proteins fused to O^6-alkylguanine-DNA alkyltransferase with enzymatic substrate derivatives and labelling of cell surface proteins tagged with a 15-amino-acid peptide through biotinylation by *Escherichia coli* biotin ligase. These techniques allow specific labelling of recombinant proteins with small organic fluorophores within live cells.

In addition to the small organic fluorophores, semiconductor nanocrystals, known as quantum dots, are among the most promising emerging fluorescent labels. Currently, quantum dots are mostly attached to the extracellular or intraluminal domains of membrane proteins. They have several advantages over organic fluorophores and FPs, including photostability and a wide range of excitation and emission wavelengths. However, the use of quantum dots has been limited by difficulties in making them fully biocompatible.

is assumed to substantially limit the lateral spreading of signalling information on the plasma membrane.

Tracking membrane-bound cytosolic proteins. Compared with transmembrane proteins or GPI-anchored proteins, cytosolic proteins are less accessible to antibodies used in labelling techniques. Because of this, membrane-bound cytosolic proteins are fused to FPs. Their binding to and lateral movement on the plasma membrane have been tracked with a high signal/background ratio by total internal reflection fluorescence microscopy (TIRFM), which uses an evanescent wave to selectively illuminate and excite fluorophores in a restricted region of the specimen immediately adjacent to the glass–water interface[88–92] (that is, a surface region, such as the basal plasma membrane). In addition, the translocation of many signalling proteins along the axial dimension can be analysed by switching the microscopy mode between TIRF and conventional epifluorescence[93,94]. Similar single-molecule imaging with a high signal/background ratio can also be achieved deep inside of cells. For example, highly inclined and laminated optical sheet (HILO) microscopy was developed to observe blinking bright spots that represent single molecules of importin-β–GFP interacting with the nuclear pore complex during nuclear transport[95].

In these experiments, photostable FPs are preferred to accomplish long-term tracking. It is thus important to explore the possibility of improving currently available FPs. Tsien's group[96] used a photostability selection method to screen libraries of mutated FPs for enhanced photostability. For example, TagRFP[97], which is reasonably photostable, has been further improved by a single mutation (Ser158Thr) to generate TagRFP-T[96]; this is the most photostable of all known FPs.

Tracking soluble cytosolic proteins. Compared with membrane-bound proteins, soluble proteins are difficult to track because they move very fast in 3D space. A similar comparison can be made between polymerized F-actin and monomeric globular actin (G-actin). As the cytoskeleton is continuously remodelled by the polymerization and depolymerization of actin, the relative content of F-actin and G-actin are subject to temporal and spatial fluctuations. F-actin can be visualized by conventional epifluorescence or TIRF microscopy, whereas G-actin cannot. Nevertheless, the rapid movement of soluble cytosolic proteins, including G-actin, can be analysed by fluorescence correlation spectroscopy (FCS). FCS enables correlation analysis of fluctuations in the fluorescence intensity in a defined illumination volume fixed in space. In this method, light is focused on a confocal volume inside a cell containing fluorescently labelled proteins, and then the fluorescence intensity fluctuations that are due to diffusion, reactions or aggregation are measured and the data analysed using a temporal autocorrelation technique[98].

Conventional FCS typically uses small organic fluorophores to label proteins of interest. However, recent progress in the application of FCS to living cells has taken particular advantage of the detection of FPs and their genetically encoded fusions to cellular proteins[99]. FCS in living cells seems to require some 'tips and tricks' to minimize artefacts, optimize measurement conditions and obtain parameter values[100]. Numerous FCS-related methods have been proposed and practised in the past decade, including multicolour applications, high spatial and temporal resolution and multiplexing[101]. It should be noted that FCS can also be used to study membrane dynamics and protein or lipid interactions.

Tracking polymeric proteins. As discussed above, the overall structures of cytoskeletal polymers, such as F-actin, can be visualized by introducing a sufficient amount of fluorescent subunits (actin–EGFP). Recently, fluorescent speckle microscopy (FSM), which was originally used to study microtubule dynamics, has been used to examine the actin cytoskeleton[102]. FSM uses low levels of fluorescent labels to create fluorescent speckles on cytoskeletal polymers in the high-resolution fluorescence imaging of living cells[103]. The dynamics of the speckles over time provides information on subunit turnover and motion of the cytoskeletal polymers. This approach has even been used to study non-polymeric macromolecular assemblies, such as focal adhesions[102].

Higher resolution tracking of single molecules. In conventional single-particle tracking studies, such as the ones mentioned above, the imaged molecular density in any single frame needs to be low because particle localization requires that the molecules be separated by a distance greater than the diffraction limit. In practice, therefore, many cells have to be observed to obtain statistically significant information about a given particle's behaviour. To overcome the diffraction barrier of light, numerous methods capable of temporally separating molecules that would otherwise be spatially indistinguishable have been developed (FIG. 3a), known as super-resolution imaging (reviewed in REFS 20,53). These include PALM[20,53,104], FPALM[20,53,105] and stochastic optical reconstruction microscopy (STORM)[106]. Among

Axial dimension
The dimension along the optical axis of an objective lens.

Highly inclined and laminated optical sheet
The illumination light for single-molecule imaging inside cells. The light is generated by positioning the incident beam to propagate near the objective edge.

Multiplexing
A method that allows the simultaneous imaging of multiple events in a single cell.

Diffraction limit
Although an ideal optical system would image an object point perfectly as a point, diffraction occurs owing to the wave-like nature of radiation, and the result is that the image of a point is a blur. Thus, the ability of an imaging system to resolve detail is ultimately limited by diffraction.

Stochastic optical reconstruction microscopy
A high-resolution fluorescence microscopy method based on high- accuracy localization of photoswitchable fluorophores.

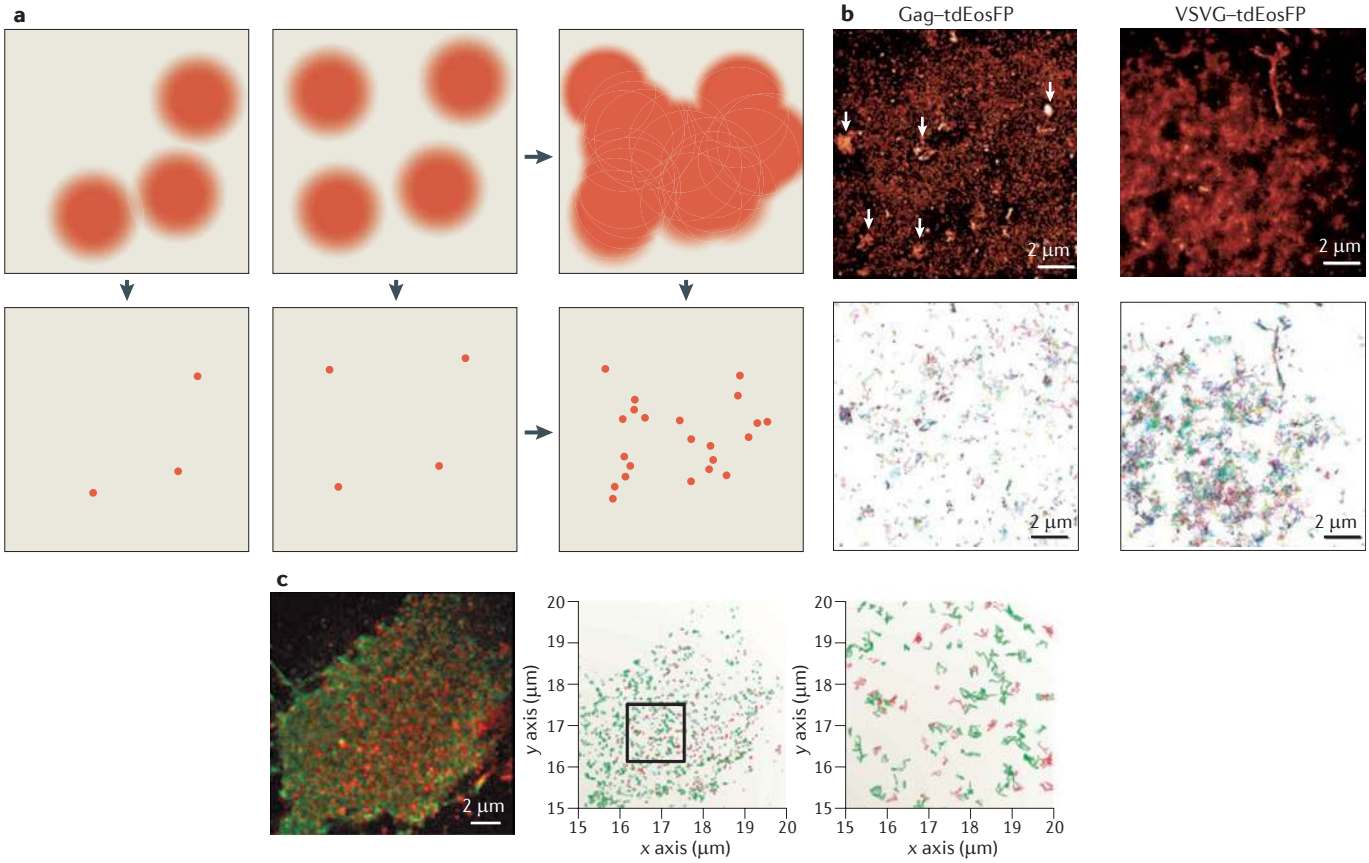

Figure 3 | **SptPALM and its dual-colourization. a** | Schematic of photoactivated localization microscopy (PALM) analysis. A densely populated specimen is illuminated with low-intensity activation light so that only a sparse pool of molecules is activated. Raw data (top) are acquired under intense excitation. The position of each molecule is localized by fitting the measured photon distribution with a two-dimensional Gaussian function (bottom). These molecules are photobleached before additional cycles of activation and photobleaching of new molecules are carried out. Combining the information obtained from the cycles (right) generates high-density, high-resolution maps with the position of each molecule. **b** | Trajectories of single molecules of the HIV-1 protein Gag or vesicular stomatitis virus glycoprotein (VSVG), both tagged with tandem dimeric Eos fluorescent protein (tdEosFP), in live COS7 cells. PALM images of Gag–tdEosFP and VSVG–tdEosFP, integrated over 500 s (10,000 images) are shown in the top panel. Single-particle tracking PALM (sptPALM) trajectories of localized Gag–tdEosFP and VSVG–tdEosFP molecules that are longer than 15 frames (750 ms) are shown in the bottom panel; each track is represented by a different colour. White arrows indicate large Gag-enriched regions. **c** | VSVG tagged to photoactivatable green FP (PA-GFP) and epidermal growth factor receptor (EGFR) tagged to PA-TagRFP (red FP) were co-expressed in COS7 cells. PALM images of VSVG–PA-GFP (green) and EGFR–PA-TagRFP (red) are merged in the left panel. Dual-colour sptPALM trajectories of localized VSVG–PA-GFP (green) and EGFR–PA-TagRFP (red) molecules that are longer than 0.7 s are shown in the middle panel. A close-up view of the region indicated by the square is shown in the right panel. Images in part **a** are reproduced, with permission, from REF. 141. Images in part **b** are reproduced, with permission, from REF. 107 © (2008) Macmillan Publishers Ltd. All rights reserved. Image in part **c** is reproduced, with permission, from REF. 57 © (2010) American Chemical Society.

these methods, PALM and FPALM use photoactivatable or photoconvertible FPs.

By combining the techniques of PALM and single-particle tracking, it is possible to resolve the dynamics of individual molecules on a scale below the diffraction limit. This new technique, called single-particle tracking PALM (sptPALM)[107], allows the localization and tracking of many overlapping trajectories because the distance between fluorescent molecules in any single frame is several times greater than the width of the point spread function (that is, the irradiance distribution that results from a single point source). The resulting high density of dynamic information can provide a spatially resolved map of single-molecule diffusion constants. Initially, sptPALM was developed to obtain information on the heterogeneity of protein movement in biological membranes. Manley *et al.*[107] applied sptPALM to live COS7 cells expressing tdEosFP fused to either the HIV-1 protein Gag or vesicular stomatitis virus glycoprotein (VSVG), two proteins known to have different distributions and mobility. They were able to obtain several orders of magnitude more trajectories per cell than had been obtainable by conventional single-particle tracking and to confirm, both intuitively and statistically, that more VSVG–tdEosFP molecules were mobile compared with Gag–tdEosFP molecules (FIG. 3b).

However, it is desirable to compare the trajectories of two different membrane-associated proteins in the same cell sample. Aiming at dual-colour sptPALM, Subach *et al.*[57] developed a monomeric, dark-to-red photoactivatable RFP, PA-TagRFP[57], which is a better partner of PA-GFP and shows better photostability than PA-mCherry. Dual-colour sptPALM imaging was achieved to monitor the dynamics of two different single transmembrane proteins fused to PA-TagRFP and PA-GFP in the same cell (FIG. 3c).

Expansion of the field of view. Unlike bulk measurements, measurements of single-molecule movement usually require that the cells or subcellular structures be loaded with only a very small amount of FP-fused proteins. Moreover, when endogenous proteins are labelled with their antibodies to be observed, no expression of exogenous proteins is required. In this case, there is no concern about the perturbation of normal cellular processes or the artefactual movement of proteins. By contrast, the antibody-labelling technique is occasionally subject to the criticism that the antibody-coated particles may crosslink the proteins to be analysed.

One drawback of measurements of single-molecule movement lies in the narrowness of the field of view. When making such observations, it is difficult to zoom out of the cell to track proteins across the entire cell or even between different compartments. In particular, the single-point fluorescence measurement of FCS yields limited information about the spatial regulation of protein movement. One way to address this issue is to double the number of measurement points, which increases the ability to acquire such information. For example, the pair correlation function (pCF) method can be used to measure the time taken by a molecule to migrate from one location to another[108]. The spatial and temporal correlation between two arbitrary points provides a local map of protein movement, such as nucleocytoplasmic transport[108].

Furthermore, more spatiotemporal information can be obtained by observing multiple points in parallel, using a confocal laser-scanning microscope (CLSM). In scanning FCS techniques[109], the measurement volume is moved across the sample in a defined way; this approach is also called image correlation spectroscopy (ICS). Its variations include raster ICS (RICS), which can extract information about molecular dynamics and concentrations from images of living cells taken on common commercial confocal systems[110]. As a new image correlation approach, a microscope was recently constructed based on light-sheet illumination to acquire FCS data in a parallelized manner[111]. Their 2D FCS imaging using 3T3 cells that expressed heterochromatin protein 1α (HP1α) tagged to EGFP, revealed the existence of regions inside euchromatin with heterochromatin-like affinity to HP1α.

Imaging protein–protein interactions

Imaging the movement (fluctuation) of proteins provides information about their interactions with other molecules and structures. For example, FCS can be used to study molecular interactions by measuring differences in diffusion times. However, diffusion-based measurements are relatively insensitive to changes in molecular mass[8]. Fluorescence cross-correlation spectroscopy (FCCS)[112] traces two spectrally distinguishable fluorophores to identify when the two molecules coincide and thus, it detects molecular interactions more sensitively than FCS. Some FPs that are endowed with large Stokes shifts, including Keima[113] and large Stokes shift mKate (LSS-mKate)[114], can be used in combination with CFP to achieve simple but efficient FCCS using a single laser beam.

More details about the spatiotemporal patterns of protein–protein interactions can be obtained by bimolecular FRET[115–120]. FRET involves the radiationless transfer of energy from an initially excited donor to an acceptor; this allows the quantification of the interacting fraction of molecules, which is also relevant to reaction–diffusion studies. In bimolecular FRET, as the donor and the acceptor are not linked covalently, they can move independently in their free forms. Because extracellular stimuli may cause protein movement (translocation or redistribution) inside cells, donor–acceptor stoichiometry in a region of interest may change substantially during an experiment. To correct for the uncertain stoichiometry, as well as other interfering parameters, three fluorescence intensity measurements (donor and acceptor emission bands following excitation of the donor band, and acceptor emission band following excitation of the acceptor) are frequently obtained in three cell samples that express donors only, acceptors only or both donors and acceptors[121–123].

However, measurement of the donor fluorescence lifetime is the most reliable method to quantify FRET efficiency. Fluorescence lifetime imaging microscopy (FLIM) is the preferred bimolecular FRET approach for quantitative equilibrium analysis because it enables quantification of the fraction of donor bound to acceptor independently of fluorophore concentration per se. Recently, two-photon FLIM was used to visualize the interactions of small GTPases and their binding partners in neurons[124,125] (FIG. 4). Specifically, this type of microscopy was used together with FRET sensors, which consisted of RAS, RHOA and CDC42 tagged with mEGFP and their respective binding partner tagged with mRFP1 or mCherry. These imaging experiments allowed the observation of the spine–shaft spreading activity of small GTPases, which contributes to neuronal plasticity. Interestingly, the spatial profiles of these molecules can be accurately described using a simple geometric model[126]. By taking into consideration the movement of other proteins that shuttle between spines and shafts, it will be possible to refine the model even further.

Bimolecular fluorescence complementation (BiFC) is a reliable tool to analyse the occurrence and subcellular localization of protein–protein interactions in live cells[18,127]. The BiFC assay is based on the reconstitution of an FP from two non-fluorescent fragments. If the two fragments are brought into close proximity through a physical interaction between the proteins fused to each fragment, the complete FP structure will be easily reconstituted, and fluorescence will be produced. Although this technique has one limitation (the irreversible association of FP fragments), it can provide temporally

Pair correlation function
A function that shows the probability of finding the centre of a particle that is located a given distance from the centre of another particle.

Euchromatin
A form of chromatin that is lightly packed and often transcriptionally active during interphase.

Heterochromatin
A condensed form of chromatin in which the degree of compaction is similar to that of mitotic chromosomes. It is usually found around the centromere.

Stokes shifts
The energy difference between the emitted photon and the absorbed photon. The Stokes shift is usually expressed as the difference between positions of the band maxima of the absorption and emission spectra.

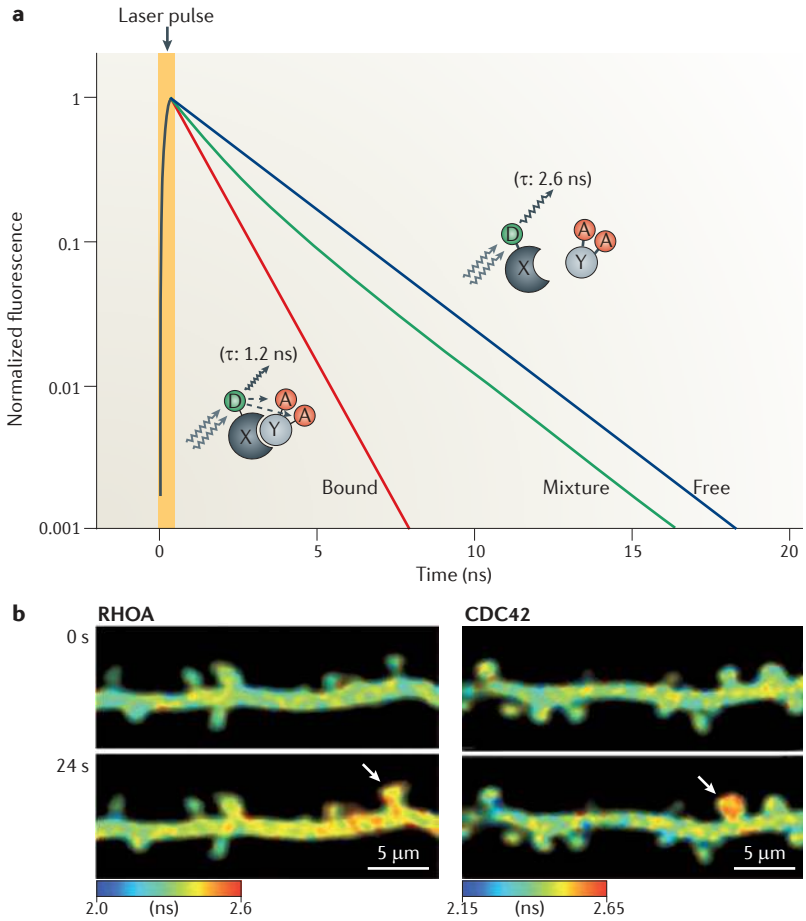

Figure 4 | **Time-domain, two-photon FLIM for monitoring the activation of small GTPases. a** | Schematic illustration of the time-domain, two-photon fluorescence lifetime imaging microscopy (FLIM) used to examine the interaction of RAS, RHOA or CDC42 (labelled X) with their respective binding partner (labelled Y). X is tagged with monomeric enhanced green fluorescent protein (mEGFP) (the donor, D), which is excited at a wavelength of 920 nm, and Y is tagged with two monomeric red FPs, mRFP or mCherry (the acceptor, A). Supposing that the excited state of mEGFP decays with time constants (τs) of 2.6 ns and 1.2 ns in the free and bound states, respectively, the time-course curve for the excited state of mEGFP can be fitted to the double exponential $F(t) \sim \alpha \exp(-t/2.6) + \beta \exp(-t/1.2)$; in which α and β are percentages of free and bound states, respectively ($\alpha + \beta = 1$), t is time and F is the normalized fluorescence intensity. Supposing, for example, that $\alpha = \beta = 0.5$, the time course (mixture, green curve) is given by $F(t) \sim 1/2\exp(-t/2.6) + 1/2\exp(-t/1.2)$. **b** | Fluorescence lifetime images of RHOA (left) and CDC42 (right) activities before (0 s) and after (24 s) glutamate uncaging (which is used to stimulate individual spines). The stimulated spines are indicated by arrows. Activation (red) of RHOA spread over the dendrites with a small gradient between the stimulated spines and dendrites; CDC42 activation was restricted to the stimulated spines. Images in part **b** are reproduced, with permission, from REF. 125 © (2011) Macmillan Publishers Ltd. All rights reserved.

integrated information of protein–protein interactions with high sensitivity. This assay is expected to allow the visualization of transient or low-affinity interactions, such as those between enzymes and substrates.

Finally, more direct information about the interaction between membrane-associated proteins can be obtained by colocalization analysis using dual-colour super-resolution imaging data. For example, dual-colour PALM using a photoconvertible FP (tdEosFP) and a photochromic FP (Dronpa or PS-CFP2) was used to resolve different pairs of proteins assembled in adhesion complexes[128]. This technology has been advanced further by the development of PA-mCherry and PA-TagRFP, which show excellent photoactivation contrast and brightness and can function as good markers together with PA-GFP for dual-colour PALM imaging. This method was used to observe that transferrin receptor and clathrin light chain fused to PA-mCherry and PA-GFP, respectively, were differentially localized to tiny clusters (~200 nm) at different maturation stages[56].

The higher resolution tracking of two different single proteins within a membrane may be a promising approach for evaluating the stability of their complexes and distinguishing substantial interactions between the two proteins from their accidental collisions. However, monitoring the joint diffusion of a pair of two different proteins is expected to be difficult because only a very small fraction of photoactivatable FPs is photoactivated in an sptPALM experiment. Because of this, the tracking of two interacting proteins is rarely achieved.

Perspectives

While studying the spatiotemporal regulation of intracellular signalling within a living cell, we witness various proteins on the move, participating in diverse chemical reactions in different locations and on different timescales[22,129]. As we improve our knowledge of protein movement in the cell, quantitative analysis of relative speed is necessary to better understand spatiotemporal regulation, as it will reveal which process limits the spatiotemporal pattern.

Currently, there is a trend towards studying protein dynamics in a physiological context. To this end, the ultimate approach would be to apply two-photon activation to an intact living organism. This was done in the study that examined the dynamics of the scaffolding protein PSD95 fused to PA-GFP within individual spines of layer 2 or 3 dendrites in the developing mouse barrel cortex[72] (see above). Owing to recent remarkable progress in gene transfer techniques, including electroporation, virus-mediated gene transfer and germline transmission of transgenes, it may be possible to use such methods in primates as well[130].

Although this Review has focused on observations of biological events occurring within a single cell, it is also important to visualize protein movement in extracellular space within larger-scale 3D structures, such as whole bodies[131]. For example, kinetic studies of how diffusion and transport of morphogen peptides are related to their binding and metabolism will clarify the mechanisms underlying the formation of morphogenic gradients in developing embryos[132]. Remarkably, modular, scanning FCCS has been developed to measure ligand–receptor affinities in living animals[133]. This was used to quantify the mobility of fibroblast growth factor (Fgf) receptor 1 (Fgfr1) and Fgfr4 fused to mRFP in the cell membranes of living zebrafish embryos and determine their *in vivo* binding affinities to their ligand, Fgf8, fused to EGFP. Also, the light-sheet illumination-based 2D FCS imaging of protein diffusion was carried out in *Drosophila melanogaster* wing imaginal discs[111].

Our understanding of protein dynamics within the cell will be improved by combining different techniques, for example the marriage of photoactivation and two-photon activation, as discussed above. Other examples that underscore the potential of combining different techniques include a combination of FRET with photoactivation (Phamret)[58] or photochromism (pcFRET)[82], single-particle tracking with PALM (sptPALM)[107], and FSM with photoconversion[134]. Needless to say, future expansion of this technology will require additional combinations of techniques.

Today, more and more researchers are taking multiple approaches to studying the dynamics of their protein of interest. We should be reminded of the study that examined the association and dissociation rates of the binding kinetics of EEA1 by photoactivation and FRAP experiments that used EEA1–PA-EGFP and EEA1–EGFP, respectively[65]. It will be important to analyse protein movement comparatively by using both bulk and single-molecule measurements. For example, it will become possible to monitor the dynamics of both F-actin and G-actin within a single dendritic spine. The two forms of actin may be analysed alternately even with different time- and length-scales. It is also important to note that the global and local diffusion processes on the cell surface, such those obtained by FRAP (or photoactivation) and FCS experiments, may be characterized by significantly different *D* values. For example, according to the fence model discussed above[87], the diffusion of a transmembrane protein in the plasma membrane may be very active within a compartment but may seem to be a slow process when measured across the entire cell. Thus, researchers should be aware of the biases inherent to the approaches they use to study protein movement.

Although the range of patterns amenable to observation is limited by the performance of current microscopy systems, there is hope that this limitation will be overcome in the future. Numerous photomodulatable FPs have been developed following the emergence of PA-GFP[12] and Kaede[13] in 2002. In each of those FPs, photoactivation or photoconversion is achieved by excitation of the protonated form of a chromophore that absorbs light maximally at approximately 400 nm (see Supplementary information S2 (figure))[135,136]. Coincidentally, the past decade has witnessed a huge expansion in the market for Blu-ray disc players, which use 405-nm diode lasers. As the lasers have become the standard light source in the industrial realm, today the norm is to equip commercial CLSM systems with similar violet-laser diodes to facilitate photoactivation–photoconversion techniques. An important consideration is that the light for photomodulation should not be limited to only violet. Green-to-red Dendra[61] and, more recently, orange-to-far-red PS-mOrange[64] can be photoconverted by blue and blue-green light, respectively, which will further diversify the utility of this technique.

With the growing popularity and use of photomodulatable FPs, the technique will continue to be refined and diversified. Newly emerging tools will surely stimulate the imagination of many biologists, and this increased interest is expected to spark an upsurge in the demand for the tools themselves. Consequently, fluorescence microscopes will need to be equipped with special hardware and software functions to optimize their use. A significant evolution in microscopy will be necessary if photoactivation–photoconversion techniques are to enjoy widespread use. Commercial microscopy systems should evolve into ones that are amenable to the addition of many new functions.

1. Tsien, R. Y. The green fluorescent protein. *Annu. Rev. Biochem.* **67**, 509–544 (1998).
2. Miyawaki, A. Innovations in the imaging of brain functions using fluorescent proteins. *Neuron* **48**, 189–199 (2005).
3. Shaner, N. C., Steinbach, P. A. & Tsien, R. Y. A guide to choosing fluorescent proteins. *Nature Methods* **2**, 905–909 (2005).
4. Lin, M. Z., Miyawaki, A. & Tsien, R. Y. Fluorescent proteins illuminate cell biology (Poster). *Nature Rev. Mol. Cell Biol.* **10** (2010).
5. Shaner, N. C., Patterson, G. H. & Davidson, M. W. Advances in fluorescent protein technology. *J. Cell Sci.* **120**, 4247–4260 (2007).
6. Day, R. N. & Davidson, M. W. The fluorescent protein palette: tools for cellular imaging. *Chem. Soc. Rev.* **38**, 2887–2921 (2009).
7. Chudakov, D. M., Matz, M. V., Lukyanov, S. & Lukyanov, K. A. Fluorescent proteins and their applications in imaging living cells and tissues. *Physiol. Rev.* **90**, 1103–1163 (2010).
8. Lippincott-Schwartz, J., Snapp, E. & Kenworthy, A. Studying protein dynamics in living cells. *Nature Rev. Mol. Cell Biol.* **2**, 444–456 (2001).
9. Yokoe, H. & Meyer, T. Spatial dynamics of GFP-tagged proteins investigated by local fluorescence enhancement. *Nature Biotech.* **14**, 1252–1256 (1996).
10. Brejc, K. *et al.* Structural basis for dual excitation and photoisomerization of the *Aequorea victoria* green fluorescent protein. *Proc. Natl Acad. Sci. USA* **94**, 2306–2311 (1997).
11. Matz, M. V. *et al.* Fluorescent proteins from nonbioluminescent Anthozoa species. *Nature Biotech.* **17**, 969–973 (1999).
12. Patterson, G. H. & Lippincott-Schwartz, J. A photoactivatable GFP for selective photolabeling of proteins and cells. *Science* **297**, 1873–1877 (2002).
13. Ando, R., Hama, H., Yamamoto-Hino, M., Mizuno, H. & Miyawaki, A. An optical marker based on the UV-induced green-to-red photoconversion of a fluorescent protein. *Proc. Natl Acad. Sci. USA* **99**, 12651–12656 (2002).
14. Phair, R. D. & Misteli, T. Kinetic modelling approaches to *in vivo* imaging. *Nature Rev. Mol. Cell Biol.* **2**, 898–907 (2001).
15. Brandizzi, F., Fricker, M. & Hawes, C. A greener world: the revolution in plant bioimaging. *Nature Rev. Mol. Cell Biol.* **3**, 520–530 (2002).
16. Zhang, J., Campbell, R. E., Ting, A. Y. & Tsien, R. Y. Creating new fluorescent probes for cell biology. *Nature Rev. Mol. Cell Biol.* **3**, 906–918 (2002).
17. Lukyanov, K. A., Chudakov, D. M., Lukyanov, S. & Verkhusha, V. V. Photoactivatable fluorescent proteins. *Nature Rev. Mol. Cell Biol.* **6**, 885–891 (2005).
18. Kerppola, T. K. Visualization of molecular interactions by fluorescence complementation. *Nature Rev. Mol. Cell Biol.* **7**, 449–456 (2006).
19. Pepperkok, R. & Ellenberg, J. High-throughput fluorescence microscopy for systems biology. *Nature Rev. Mol. Cell Biol.* **7**, 690–696 (2006).
20. Fernández-Suárez, M. & Ting, A. Y. Fluorescent probes for super-resolution imaging in living cells. *Nature Rev. Mol. Cell Biol.* **9**, 929–943 (2008).
21. Shav-Tal, Y., Singer, R. H. & Darzacq, X. Imaging gene expression in single living cells. *Nature Rev. Mol. Cell Biol.* **5**, 855–861 (2004).
22. Dehmelt, L. & Bastiaens, P. I. Spatial organization of intracellular communication: insights from imaging. *Nature Rev. Mol. Cell Biol.* **11**, 440–452 (2010).
23. Yang, M., Jiang, P. & Hoffman, R. M. Whole-body subcellular multicolor imaging of tumor-host interaction and drug response in real time. *Cancer Res.* **67**, 5195–5200 (2007).
24. Nowotschin, S., Eakin, G. S. & Hadjantonakis, A. K. Live-imaging fluorescent proteins in mouse embryos: multi-dimensional, multi-spectral perspectives. *Trends Biotechnol.* **27**, 266–276 (2009).
25. Chudakov, D. M., Lukyanov, S. & Lukyanov, K. A. Fluorescent proteins as a toolkit for *in vivo* imaging. *Trends Biotechnol.* **23**, 605–613 (2005).
26. Labas, Y. A. *et al.* Diversity and evolution of the green fluorescent protein family. *Proc. Natl Acad. Sci. USA* **99**, 4256–4261 (2002).
27. Matz, M. V., Lukyanov, K. A. & Lukyanov, S. A. Family of the green fluorescent protein: journey to the end of the rainbow. *Bioessays* **24**, 953–959 (2002).
28. Shagin, D. A. *et al.* GFP-like proteins as ubiquitous metazoan superfamily: evolution of functional features and structural complexity. *Mol. Biol. Evol.* **21**, 841–850 (2004).
29. Zacharias, D. A., Violin, J. D., Newton, A. C. & Tsien, R. Y. Partitioning of lipid-modified monomeric GFPs into membrane microdomains of live cells. *Science* **296**, 913–916 (2002).
30. Campbell, R. E. *et al.* A monomeric red fluorescent protein. *Proc. Natl Acad. Sci. USA* **99**, 7877–7882 (2002).
31. Wall, M. A., Socolich, M. & Ranganathan, R. The structural basis for red fluorescence in the tetrameric GFP homolog DsRed. *Nature Struct. Biol.* **7**, 1133–1138 (2000).

32. Yarbrough, D., Wachter, R. M., Kallio, K., Matz, M. V. & Remington, S. J. Refined crystal structure of DsRed, a red fluorescent protein from coral, at 2.0-Å resolution. *Proc. Natl Acad. Sci. USA* **98**, 462–467 (2001).
33. Shaner, N. C. *et al.* Improved monomeric red, orange and yellow fluorescent proteins derived from *Discosoma* sp. red fluorescent protein. *Nature Biotech.* **22**, 1567–1572 (2004).
34. Wiedenmann, J. *et al.* EosFP, a fluorescent marker protein with UV-inducible green-to-red fluorescence conversion *Proc. Natl Acad. Sci. USA* **101**, 15905–15910 (2004).
35. Yanushevich, Y. G. *et al.* A strategy for the generation of non-aggregating mutants of Anthozoa fluorescent proteins. *FEBS Lett.* **511**, 11–14 (2002).
36. Katayama, H., Yamamoto, A., Yoshimori, T., Mizushima, N. & Miyawaki, A. GFP-like proteins stably accumulate in lysosomes. *Cell Struct. Funct.* **33**, 1–12 (2008).
37. Tsutsui, H., Karasawa, S., Shimizu, H., Nukina, N. & Miyawaki, A. Semi-rational engineering of a coral fluorescent protein into an efficient highlighter. *EMBO Rep.* **6**, 233–238 (2005).
38. Shimozono, S., Tsutsui, H. & Miyawaki, A. Diffusion of large molecules into assembling nuclei revealed using an optical highlighting techniques. *Biophys. J.* **97**, 1288–1294 (2009).
39. Lauf, U., Lopez, P. & Falk, M. M. Expression of fluorescently tagged connexins, a novel approach to rescue function of oligomeric DsRed-tagged proteins. *FEBS Lett.* **498**, 11–15 (2001).
40. Bulina, M. E., Verkhusha, V. V., Staroverov, D. B., Chudakov, D. M. & Lukyanov, K. A. Hetero-oligomeric tagging diminishes non-specific aggregation of target proteins fused with Anthozoa fluorescent proteins. *Biochem. J.* **371**, 109–114 (2003).
41. Axelrod, D., Koppel, D. E., Schlessinger, J., Elson, E. & Webb, W. W. Mobility measurement by analysis of fluorescence photobleaching recovery kinetics. *Biophys. J.* **16**, 1055–1069 (1976).
42. Jacobson, K. A. *et al.* Cellular determinants of the lateral mobility of neural cell adhesion molecules. *Biochim. Biophys. Acta* **1330**, 138–144 (1997).
43. Ellenberg, J. *et al.* Nuclear membrane dynamics and reassembly in living cells: targeting of an inner nuclear membrane protein in interphase and mitosis. *J. Cell Biol.* **138**, 1193–1206 (1997).
44. Sprague, B. L. & McNally, J. G. FRAP analysis of binding: proper and fitting. *Trends Cell Biol.* **15**, 84–91 (2005).
45. Rabut, G. & Ellenberg, J. in *Live Cell Imaging* (eds Goldman, R. D. & Spector, D. L.) 101–127 (Cold Spring Harbor Laboratory Press, New York, 2005).
46. Cole, N. B. *et al.* Diffusional mobility of Golgi proteins in membranes of living cells. *Science* **273**, 797–801 (1996).
47. Kohler, R. H., Cao, J., Zipfel, W. R., Webb, W. W. & Hanson, M. R. Exchange of protein molecules through connections between higher plant plastids. *Science* **276**, 2039–2042 (1997).
48. Zaal, K. J. *et al.* Golgi membranes are absorbed into and remerge from the ER during mitosis. *Cell* **99**, 589–601 (1999).
49. Kruhlak, M. J. *et al.* Reduced mobility of the alternate splicing factor (ASF) through the nucleoplasm and steady state speckle compartments. *J. Cell Biol.* **150**, 41–51 (2000).
50. Swaminathan, R., Hoang, C. P. & Verkman, A. S. Photobleaching recovery and anisotropy decay of green fluorescent protein GFP-S65T in solution and cells: cytoplasmic viscosity probed by green fluorescent protein translational and rotational diffusion. *Biophys. J.* **72**, 1900–1907 (1997).
51. Partikian, A., Olveczky, B., Swaminathan, R., Li, Y. & Verkman, A. S. Rapid diffusion of green fluorescent protein in the mitochondrial matrix. *J. Cell Biol.* **140**, 821–829 (1998).
52. Dayel, M. J., Hom, E. F. Y. & Verkman, A. S. Diffusion of green fluorescent protein in the aqueous-phase lumen of endoplasmic reticulum. *Biophys. J.* **76**, 2843–2851 (1999).
53. Lippincott-Schwartz, J. & Patterson, G. H. Photoactivatable fluorescent proteins for diffraction-limited and super-resolution imaging. *Trends Cell Biol.* **19**, 555–565 (2009).
54. Sample, V., Newman, R. H. & Zhang, J. The structure and function of fluorescent proteins. *Chem. Soc. Rev.* **38**, 2582–2864 (2009).
55. Verkhusha, V. V. & Sorkin, A. Conversion of the monomeric red fluorescent protein into a photoactivatable probe. *Chem. Biol.* **12**, 279–285 (2005).
56. Subach, F. V. *et al.* Photoactivatable mCherry for high-resolution two-color fluorescence microscopy. *Nature Methods* **6**, 153–159 (2009).
57. Subach, F. V., Patterson, G. H., Renz, M., Lippincott-Schwartz, J. & Verkhusha, V. V. Bright monomeric photoactivatable red fluorescent protein for two-color super-resolution sptPALM of live cells. *J. Am. Chem. Soc.* **132**, 6481–6491 (2010).
58. Matsuda, T., Miyawaki, A. & Nagai, T. Direct measurement of protein dynamics inside cells using a rationally designed photoconvertible protein. *Nature Methods* **5**, 339–345 (2008).
59. McKinney, S. A., Murphy, C. S., Hazelwood, K. L., Davidson, M. W. & Looger, L. L. A bright and photostable photoconvertible fluorescent protein. *Nature Methods* **6**, 131–133 (2009).
60. Habuchi, S., Tsutsui, H., Kochaniak, A. B., Miyawaki, A. & van Oijen, A. M. mKikGR, a monomeric photoswitchable fluorescent protein. *PloS ONE* **3**, e3944 (2008).
61. Gurskaya, N. G. *et al.* Engineering of a monomeric green-to-red photoactivatable fluorescent protein induced by blue light. *Nature Biotech.* **24**, 461–465 (2006).
62. Fuchs, J. *et al.* A photoactivatable marker protein for pulse-chase imaging with superresolution. *Nature Methods* **7**, 627–630 (2010).
63. Chudakov, D. M. *et al.* Photoswitchable cyan fluorescent protein for protein tracking. *Nature Biotech.* **22**, 1435–1439 (2004).
64. Subach, O. M. *et al.* A photoswitchable orange-to-far-red fluorescent protein, PSmOrange. *Nature Methods* **8**, 771–777 (2011).
65. Bergeland, T., Haugen, L., Landsverk, O. J., Stenmark, H. & Bakke, O. Cell-cycle-dependent binding kinetics for the early endosomal tethering factor EEA1. *EMBO Rep.* **9**, 171–178 (2008).
66. Plachta, N., Bollenbach, T., Pease, S., Fraser, S. E. & Pantazis, P. Oct4 kinetics predict cell lineage patterning in the early mammalian embryo. *Nature Cell Biol.* **13**, 117–123 (2011).
67. Svoboda, K., Tank, D. W. & Denk, W. Direct measurement of coupling between dendritic spines and shafts. *Science* **272**, 716–719 (1996).
68. Helmchen, F. & Denk, W. Deep tissue two-photon microscopy. *Nature Methods* **2**, 932–940 (2005).
69. Brown, E. B., Wu, E. S., Zipfel, W. & Webb, W. W. Measurement of molecular diffusion in solution by multiphoton fluorescence photobleaching recovery. *Biophys. J.* **77**, 2837–2849 (1999).
70. Star, E. N., Kwiatkowski, D. J. & Murthy, V. N. Rapid turnover of actin in dendritic spines and its regulation by activity. *Nature Neurosci.* **5**, 239–246 (2002).
71. Honkura, N., Matsuzaki, M., Noguchi, J., Ellis-Davies, G. C. & Kasai, H. The subspine organization of actin fibers regulates the structure and plasticity of dendritic spines. *Neuron* **57**, 719–729 (2008).
72. Gray, N. W., Weimer, R. M., Bureau, I. & Svoboda, K. Rapid redistribution of synaptic PSD-95 in the neocortex *in vivo*. *PLoS Biol.* **4**, e370 (2006).
73. Sturgill, J. F., Steiner, P., Czervionke, B. L. & Sabatini, B. L. Distinct domains within PSD-95 mediate synaptic incorporation, stabilization, and activity-dependent trafficking. *J. Neurosci.* **29**, 12845–12854 (2009).
74. Lukyanov, K. A. *et al.* Natural animal coloration can be determined by a nonfluorescent green fluorescent protein homolog. *J. Biol. Chem.* **275**, 25879–25882 (2000).
75. Chudakov, D. M. *et al.* Kindling fluorescent proteins for precise *in vivo* photolabeling. *Nature Biotech.* **21**, 191–194 (2003).
76. Ando, R., Mizuno, H. & Miyawaki, A. Regulated fast nucleocytoplasmic shuttling observed by reversible protein highlighting. *Science* **306**, 1370–1373 (2004).
77. Ando, R., Flors, C., Mizuno, H., Hofkens, J. & Miyawaki, A. Highlighted generation of fluorescence signals using simultaneous two-color irradiation on Dronpa mutants. *Biophys. J.* **92**, L97–L99 (2007).
78. Brakemann, T. *et al.* Molecular basis of the light-driven switching of the photochromic fluorescent protein Padron. *J. Biol. Chem.* **285**, 14603–14609 (2010).
79. Henderson, J. N., Ai, H. W., Campbell, R. E. & Remington, S. J. Structural basis for reversible photobleaching of a green fluorescent protein homologue. *Proc. Natl Acad. Sci. USA* **104**, 6672–6677 (2007).
80. Adam, V. *et al.* Structural characterization of IrisFP, an optical highlighter undergoing multiple photo-induced transformations. *Proc. Natl Acad. Sci. USA* **105**, 18343–18348 (2008).
81. Stiel, A. C. *et al.* Generation of monomeric reversibly switchable red fluorescent proteins for far-field fluorescence nanoscopy. *Biophys. J.* **95**, 2989–2997 (2008).
82. Subach, F. V. *et al.* Red fluorescent protein with reversibly photoswitchable absorbance for photochromic FRET. *Chem. Biol.* **17**, 745–755 (2010).
83. Sawano, A., Takayama, S., Matsuda, M. & Miyawaki, A. Lateral propagation of EGF signaling after local stimulation is dependent on receptor density. *Dev. Cell* **3**, 245–257 (2002).
84. Miyawaki, A. Visualization of the spatial and temporal dynamics of intracellular signaling. *Dev. Cell* **4**, 295–305 (2003).
85. Sheetz, M. P., Turney, S., Qian, H. & Elson, E. L. Nanometre-level analysis demonstrates that lipid flow does not drive membrane glycoprotein movements. *Nature* **340**, 284–288 (1989).
86. Schmidt, T., Schütz, G. J., Baumgartner, W., Gruber, H. J. & Schindler, H. Imaging of single molecule diffusion. *Proc. Natl Acad. Sci. USA* **93**, 2926–2929 (1996).
87. Kusumi, A., Shirai, Y. M., Koyama-Honda, I., Suzuki, K. G. & Fujiwara, T. K. Hierarchical organization of the plasma membrane: investigations by single-molecule tracking vs. fluorescence correlation spectroscopy. *FEBS Lett.* **584**, 1814–1823 (2010).
88. Tokunaga, M., Kitamura, K., Saito, K., Iwane, A. H. & Yanagida, T. Single molecule imaging of fluorophores and enzymatic reactions achieved by objective-type total internal reflection fluorescence microscopy. *Biochem. Biophys. Res. Commun.* **235**, 47–53 (1997).
89. Mashanov, G. I., Tacon, D., Knight, A. E., Peckham, M. & Molloy, J. E. Visualizing single molecules inside living cells using total internal reflection fluorescence microscopy. *Methods* **29**, 142–152 (2003).
90. Schneckenburger, H. Total internal reflection fluorescence microscopy: technical innovations and novel applications. *Curr. Opin. Biotechnol.* **16**, 13–18 (2005).
91. Axelrod, D. Total internal reflection fluorescence microscopy. *Methods Cell Biol.* **89**, 169–221 (2008).
92. Toomre, D. & Bewersdorf, J. A new wave of cellular imaging. *Annu. Rev. Cell Dev. Biol.* **26**, 285–314 (2010).
93. Toomre, D., Steyer, J. A., Keller, P., Almers, W. & Simons, K. Fusion of constitutive membrane traffic with the cell surface observed by evanescent wave microscopy. *J. Cell Biol.* **149**, 33–40 (2000).
94. Merrifield, C. J., Feldman, M. E., Wan, L. & Almers, W. Imaging actin and dynamin recruitment during invagination of single clathrin-coated pits. *Nature Cell Biol.* **4**, 691–698 (2002).
95. Tokunaga, M., Imamoto, N. & Sakata-Spgawa, K. Highly inclined thin illumination enables clear single-molecule imaging in cells. *Nature Methods* **5**, 159–161 (2008).
96. Shaner, N. C. *et al.* Improving the photostability of bright monomeric orange and red fluorescent proteins. *Nature Methods* **5**, 545–551 (2008).
97. Merzlyak, E. M. *et al.* Bright monomeric red fluorescent protein with an extended fluorescence lifetime. *Nature Methods* **4**, 555–557 (2007).
98. Chen, H., Farkas, E. R. & Watt, W. W. *In vivo* applications of fluorescence correlation spectroscopy. *Methods Cell Biol.* **89**, 3–35 (2008).
99. Kohl, T. & Schwille, P. Fluorescence correlation spectroscopy with autofluorescent proteins. *Adv. Biochem. Eng. Biotechnol.* **95**, 107–142 (2005).
100. Kim, S. A., Heinze, K. G. & Schwille, P. Fluorescence correlation spectroscopy in living cells. *Nature Methods* **4**, 963–973 (2007).
101. Haustein, E. & Schwille, P. Fluorescence correlation spectroscopy: novel variations of an established technique. *Annu. Rev. Biophys. Biomol. Struct.* **36**, 151–169 (2007).
102. Adams, M. C. *et al.* Signal analysis of total internal reflection fluorescent speckle microscopy (TIR-FSM) and wide-field epi-fluorescence FSM of the actin cytoskeleton and focal adhesions in living cells. *J. Microsc.* **216**, 138–152 (2004).

103. Danuser, G. & Waterman-Storer, C. M. Quantitative fluorescent speckle microscopy of cytoskeleton dynamics. *Annu. Rev. Biophys. Biomol. Struct.* **35**, 361–387 (2006).
104. Betzig, E. *et al.* Imaging intracellular fluorescent proteins at nanometer resolution. *Science* **313**, 1642–1645 (2006).
105. Hess, S. T., Girirajan, T. P. & Mason, M. D. Ultra-high resolution imaging by fluorescence photoactivation localization microscopy. *Biophys. J.* **91**, 4258–4272 (2006).
106. Rust, M. J., Bates, M. & Zhuang, X. Sub-diffraction-limit imaging by stochastic optical reconstruction microscopy (STORM). *Nature Methods* **3**, 793–795 (2006).
107. Manley, S. *et al.* High-density mapping of single-molecule trajectories with photoactivated localization microscopy. *Nature Methods* **5**, 155–157 (2008).
108. Cardarelli, F. & Gratton, E. *In vivo* imaging of single-molecule translocation through nuclear pore complexes by pair correlation functions. *PLoS ONE* **5**, e10475 (2010).
109. Petersen, N. O., Höddelius, P. L., Wiseman, P. W., Seger, O. & Magnusson, K. E. Quantitation of membrane receptor distributions by image correlation spectroscopy: concept and application. *Biophys. J.* **65**, 1135–1146 (1993).
110. Brown, C. M. *et al.* Raster image correlation spectroscopy (RICS) for measuring fast protein dynamics and concentrations with a commercial laser scanning confocal microscope. *J. Microsc.* **229**, 78–91 (2008).
111. Capoulade, J., Wachsmuth, M., Hufnagel, L. & Knop, M. Quantitative fluorescence imaging of protein diffusion and interaction in living cells. *Nature Biotech.* 7 Aug 2011 (doi:10.1038/nbt.1928).
112. Kohl, T., Haustein, E. & Schwille, P. Determining protease activity *in vivo* by fluorescence cross-correlation analysis. *Biophys. J.* **89**, 2770–2782 (2005).
113. Kogure, T. *et al.* A fluorescent variant of a protein from the stony coral *Montipora* facilitates dual-color single-laser fluorescence cross-correlation spectroscopy. *Nature Biotech.* **24**, 577–581 (2006).
114. Piatkevich, K. D. *et al.* Monomeric red fluorescent proteins with a large Stokes shift. *Proc. Natl Acd. Sci. USA* **107**, 5369–5374 (2010).
115. Miyawaki, A. & Tsien, R. Y. Monitoring protein conformations and interactions by fluorescence resonance energy transfer between mutants of green fluorescent protein. *Methods Enzymol.* **327**, 472–500 (2000).
116. Jares-Erijman, E. A. & Jovin, T. M. FRET imaging. *Nature Biotech.* **21**, 1387–1395 (2003).
117. Jares-Erijman, E. A. & Jovin, T. M. Imaging molecular interactions in living cells by FRET microscopy. *Curr. Opin. Chem. Biol.* **10**, 409–416 (2006).
118. Piston, D. W. & Kremers, G. J. Fluorescent protein FRET: the good, the bad and ugly. *Trends Biochem. Sci.* **32**, 407–414 (2007).
119. Frommer, W. B., Davidson, M. W. & Campbell, R. E. Genetically encoded biosensors based on engineered fluorescent proteins. *Chem. Soc. Rev.* **38**, 2833–2841 (2009).
120. Miyawaki, A. Development of probes for cellular functions using fluorescent proteins and fluorescence resonance energy transfer. *Annu. Rev. Biochem.* **80**, 357–373 (2011).
121. Gordon, G. W., Berry, G., Liang, X. H., Levine, B. & Herman, B. Quantitative fluorescence energy transfer measurements using fluorescence microscopy. *Biophys. J.* **74**, 2702–2713 (1998).
122. Erickson, M. G., Liang, H., Mori, M. X. & Yue, D. T. FRET two-hybrid mapping reveals function and location of L-type Ca^{2+} channel CaM preassociation. *Neuron* **39**, 97–107 (2003).
123. Berney, C. & Danuser, G. FRET or no FRET: a quantitative comparison. *Biophys. J.* **84**, 3992–4010 (2003).
124. Yasuda, R. *et al.* Supersensitive Ras activation in dendrites and spines revealed by two-photon fluorescence lifetime imaging. *Nature Neurosci.* **9**, 283–291 (2006).
125. Murakoshi, H., Wang, H. & Yasuda, R. Local, persistent activation of Rho GTPases during plasticity of single dendritic spines. *Nature* **472**, 100–104 (2011).
126. Yasuda, R. & Murakoshi, H. The mechanisms underlying the spatial spreading of signaling activity. *Curr. Opin. Neurobiol.* **21**, 313–321 (2011).
127. Kerppola, T. K. Visualization of molecular interactions using bimolecular fluorescence complementation analysis: characteristics of protein fragment complementation. *Chem. Soc. Rev.* **38**, 2876–2886 (2009).
128. Shroff, H. *et al.* Dual-color superresolution imaging of genetically expressed probes within individual adhesion complexes. *Proc. Natl Acad. Sci. USA* **104**, 20308–20313 (2007).
129. Grecco, H. E., Schmick, M. & Bastiaens, P. I. Signaling from the living plasma membrane. *Cell* **144**, 897–909 (2011).
130. Sasaki, E. *et al.* Generation of transgenic non-human primates with germline transmission. *Nature* **459**, 523–527 (2009).
131. Perentes, J. Y. *et al. In vivo* imaging of extracellular matrix remodeling by tumor-associated fibroblasts. *Nature Methods.* **6**, 143–145 (2009).
132. Harvey, S. A. & Smith, J. C. Visualisation and quantification of morphogen gradient formation in the zebrafish. *PLoS Biol.* **7**, e1000101 (2009).
133. Ries, J., Yu, S. R., Burkhardt, M., Brand, M. & Schwille, P. Modular scanning FCS quantifies receptor–ligand interactions in living multicellular organisms. *Nature Methods* **6**, 643–645 (2009).
134. Burnette, D. T. *et al.* A role for actin arcs in the leading-edge advance of migrating cells. *Nature Cell Biol.* **13**, 371–381 (2011).
135. van Thor, J. J., Gensch, T., Hellingwerf, K. J. & Johnson, L. N. Phototransformation of green fluorescent protein with UV and visible light leads to decarboxylation of glutamate 222. *Nature Struct. Biol.* **9**, 37–41 (2002).
136. Mizuno, H. *et al.* Photo-induced peptide cleavage in the green-to-red conversion of a fluorescent protein. *Mol. Cell* **12**, 1051–1058 (2003).
137. Periasamy, N. & Verkman, A. S. Analysis of fluorophore diffusion by continuous distributions of diffusion coefficients: application to photobleaching measurements of multicomponent and anomalous diffusion. *Biophys. J.* **75**, 557–567 (1998).
138. Malchus, N. & Weiss, M. Anomalous diffusion reports on the interaction of misfolded proteins with the quality control machinery in the endoplasmic reticulum. *Biophys. J.* **99**, 1321–1328 (2010).
139. Bancaud, A. *et al.* Molecular crowding affects diffusion and binding of nuclear proteins in heterochromatin and reveals the fractal organization of chromatin. *EMBO J.* **28**, 3785–3798 (2009).
140. Marks, K. M. & Nolan, G. P. Chemical labeling strategies for cell biology. *Nature Methods* **3**, 591–596 (2006).
141. Manley, S. Gillete, J. & Lippincott-Scwartz, J. Single-particle tracking photoactivated localization microscopy for mapping single-molecule dynamics. *Methods Enzymol.* **475**, 109–120 (2010).

Acknowledgements
I thank S. Shimozono and R. Ando for the images in figures 2d and 2h; H. Sakurai, V. Lakshmanam and T. Fukano for general assistance; and S. Trowbridge, D. Mou, V. Verkhusha and S. Manley for valuable comments.

Competing interests statement
The author declares no competing financial interests.

SUPPLEMENTARY INFORMATION
See online article: S1 (figure) | S2 (figure)
ALL LINKS ARE ACTIVE IN THE ONLINE PDF